Acta Cryst. (1999). A**55**, 30–47

Influence of intermolecular interactions on multipole-refined electron densities

Mark A. Spackman,[a]* Patrick G. Byrom,[a] Maria Alfredsson[b] and Kersti Hermansson[b]

[a]*Division of Chemistry, University of New England, Armidale, NSW 2351, Australia, and* [b]*Institute of Chemistry, Uppsala University, Box 531, S-751 21 Uppsala, Sweden. E-mail: mspackma@metz.une.edu.au*

(*Received 29 October 1997; accepted 19 May 1998*)

Abstract

This work examines the effect of intermolecular interactions on molecular properties derived from simulated X-ray diffraction data. Model X-ray data are computed from a superposition of *ab initio* molecular electron densities in the crystal, as well as from periodic crystal Hartree–Fock electron densities, for the hydrogen-bonded systems ice VIII, formamide and urea, as well as the weakly bound acetylene. The effects of intermolecular interactions on the electron density are illustrated at both infinite and finite data resolution, and it is concluded that multipole models are capable of quantitative retrieval of the interaction density, despite the known shortcomings of the radial functions in the model. Multipole refinement reveals considerable enhancement of the molecular dipole moment for hydrogen-bonded crystals, and negligible change in molecular second moments. Electric field gradients at H nuclei are significantly reduced in magnitude upon hydrogen bonding, and this change is also faithfully represented by the rigid pseudoatom model.

1. Introduction

In a comprehensive review of electric moments of molecules determined from X-ray diffraction data, it was asserted that 'the magnitude of the dipole moment is reliably determined and clearly demonstrates the effects of intermolecular interactions in the crystal' (Spackman, 1992). That conclusion was based on a considerable amount of experimental evidence, where standard errors in the derived moments are often large; the present work aims to test the veracity of that assertion in the case of perfect data. In addition, our working strategy allows us to broaden our scope, and we also address the effect of intermolecular interactions on molecular second and quadrupole moments, electric field gradients (EFGs) at C, N, O and H nuclei, as well as the more fundamental question of the contribution of such interactions to the structure factors and electron densities.

Because an earlier study (Spackman & Byrom, 1996) benchmarked the retrieval of the electron distribution and associated properties for a superposition of non-interacting molecules in the crystal, the present work can be described simply as a model exercise in the retrieval of the 'interaction density', defined as the difference between the electron density of the crystal and that arising from a superposition of isolated molecules, positioned as in the crystal. Of course, many other issues are involved, for instance the question of whether or not the present multipole models can retrieve *known* molecular properties, but in this work we are most interested in the differences between a superposition of molecules and a crystal, especially with respect to the following two questions:

(*a*) What are the effects of intermolecular interactions, especially hydrogen bonding, on the electron density in the crystal and the observable structure factors?

(*b*) Are these effects likely to be measurable in an experiment or observable in a multipole refinement of the electron density?

To some degree, both of these questions have been addressed previously. For example, the IUCr project on oxalic acid dihydrate (Coppens *et al.*, 1984) reported results from four different X-ray charge-density studies on that system, comparing them with theoretical results for isolated molecules; the largest differences occurred in the lone-pair regions, in qualitative agreement with the anticipated effects of hydrogen bonding. This rearrangement of the electron distribution was confirmed in detailed theoretical calculations on the water dimer by Hermansson (1985) and Krijn & Feil (1988*a*). Detailed comparisons between experimental and quantum-mechanical electron densities have also been reported for $LiOH \cdot H_2O$ (Hermansson & Lunell, 1982; Ojamäe, Hermansson, Pisani *et al.*, 1994) and for oxalic acid dihydrate (Krijn & Feil, 1988*b*; Krijn *et al.*, 1988), and of particular importance in the latter studies was the observation that agreement between experiment and theory was improved significantly when the effects of hydrogen bonding and the crystal environment were included in the theoretical model.

With the more recent availability of crystal Hartree–Fock calculations for molecular crystals (Dovesi *et al.*, 1990, 1992), the interaction density has received additional attention. In their study of urea, Dovesi *et al.* (1990) considered carefully the question of the experi-

ISSN 0108-7673

mental observability of the interaction density, and concluded that errors in experimental electron density maps [a best estimate of approximately 0.05 e $Å^{-3}$ has been reported (Krijn *et al.*, 1988)] are at present of approximately the same magnitude as the interaction density. As we shall demonstrate below, although this is a reasonable comment, it ignores the fact that the interaction density is not a random effect, but rather a systematic one, which should therefore be more amenable to observation under appropriate conditions. Recent crystal Hartree–Fock studies on urea (Gatti *et al.*, 1994), ice VIII (Gatti *et al.*, 1995) and hydrogen cyanide (Platts & Howard, 1996) have employed Bader's quantum theory of atoms in molecules (QTAM) (Bader, 1990) to analyse the effects of hydrogen bonding on molecular properties, and the conclusions therein regarding the enhancement of the dipole moment are relevant to our results reported below.

In summary, there is little doubt that the effects of hydrogen bonding are indeed in evidence in a carefully measured and derived experimental electron density for a hydrogen-bonded crystal. In order to exploit this valuable information, there is a need to examine several more model systems theoretically in order to quantify these effects. With this in mind, in this paper we study a variety of molecular crystals, including an example lacking hydrogen bonding; we also determine to what extent these interactions affect the multipole-derived molecular properties. As outlined previously (Spackman & Byrom, 1996), our strategy is simple and is summarized in flowchart fashion in Fig. 1. For this study, we specifically include intermolecular interactions and construct two different data sets: one from a model of non-interacting molecules superimposed as they occur in the crystal, and one from a Hartree–Fock wavefunction for the crystal using the same geometry and basis set. Static structure factors were computed, to a maximum $\sin\theta/\lambda = 1.0$ $Å^{-1}$, and these data sets were compared with one another, analysed with three different multipole models of varying sophistication, and these multipole model results for molecules and the crystal compared with one another. Finally, from the multipole functions, we computed molecular dipole moments, quadrupole and second moments, as well as EFGs at each nuclear site, comparing these results with those obtained from the original *ab initio* wavefunctions.

2. Computational procedure

Four molecular crystals were examined in this study (Table 1), spanning a range of bonding types (from weak van der Waals – acetylene – to strong hydrogen bonding – urea) and the three hydrogen-bonded systems have been the subject of previous theoretical crystal Hartree–Fock studies. For each molecule, a reference electron distribution was generated from an *ab initio* self-consistent field calculation, using the cell data and fractional coordinates in Table 1. As reported earlier (Spackman & Byrom, 1996), the *GAMESS* suite of programs (Schmidt *et al.*, 1993) was used with a polarized double-zeta basis set (Thakkar *et al.*, 1993). The *ab initio* derived dipole moments, second moments and EFGs were used as reference values in our subsequent comparisons with the results from the various multipole refinements. Crystal Hartree–Fock calculations, using an identical geometry and basis set to the molecular calculations, used *CRYSTAL*95 (Dovesi *et al.*, 1996), and yielded reference electron distributions and EFGs for the crystal. The crystal (per unit cell) and molecular energies are also reported in Table 1, and together these

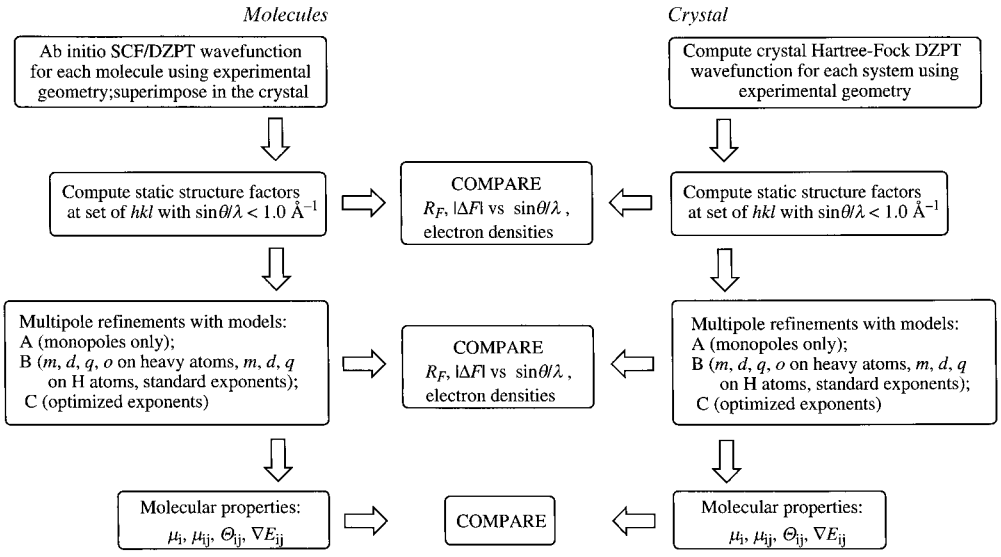

Fig. 1. A summary of the computational procedure.

Table 1. *Structural and crystallographic data for the systems studied*

	Ice VIII†	Acetylene	Formamide‡	Urea
Structure reference	Neutron, 10 K (Kuhs *et al.*, 1984)	Neutron, 131 K (McMullan *et al.*, 1992)	X-ray, 90 K (Stevens, 1978)	Neutron, 123 K (Swaminathan *et al.*, 1984)
Space group	$I4_1/amd$	$Pa\bar{3}$	$P2_1/c$	$P\bar{4}2_1m$
Z	8	4	4	2
$F(000)$	80	56	96	64
Lattice parameters	$a = b = 4.656$, $c = 6.775$ Å	$a = b = c = 6.094$ Å	$a = 6.994$, $b = 9.041$, $c = 7.261$ Å, $\beta = 150.79°$	$a = b = 5.584$, $c = 4.689$ Å
Cell volume (Å^3)	146.9	226.3	224.1	146.2
Atomic fractional coordinates	O (0, 0.25, 0.1071)	C (0.0562, 0.0562, 0.0562)	O (−0.2233, −0.0684, −0.4718)	C (0, 0.5, 0.3280)
	H (0, 0.4157, 0.1935)	H (0.1524, 0.1524, 0.1524)	N (−0.1800, 0.1570, −0.2981)	O (0, 0.5, 0.5962)
			C (−0.0769, 0.0564, −0.3350)	N (0.1447, 0.6447, 0.1785)
			H1 (−0.049, 0.256, −0.192)	H1 (0.2557, 0.7557, 0.2841)
			H2 (−0.390, 0.131, −0.383)	H2 (0.1431, 0.6431, −0.0348)
			H3 (0.146, 0.090, −0.246)	
H···O bond lengths (Å)	1.91		1.90, 1.94	2.01, 2.07
Number of reflections, N_{obs}	182	318	1874	402
ΔE (per molecule)§ (kJ mol^{-1})	−39.0	−3.3	−53.8	−79.8

† For the *CRYSTAL* calculation, cell constants and fractional coordinates were transformed to a primitive cell occupying half the volume of the body-centred cell. ‡ Cell constants and fractional coordinates have been transformed from $P2_1/n$ (cell choice 2) to $P2_1/c$ (cell choice 1) using the transformation on p. 76 of *International Tables for Crystallography* (Arnold, 1989). § The molecular binding energy is the difference between the crystal Hartree–Fock unit-cell energy divided by Z and the Hartree–Fock energy for an isolated molecule at the same geometry, using the same basis set.

enable the estimation of a lattice energy (per molecule). These estimates, also given in Table 1, ignore effects such as relaxation of the molecules in the gas phase, basis-set superposition error (BSSE), electron correlation, zero-point energies and temperature dependence. Nevertheless, the values are in accord with results reported elsewhere for ice VIII (Ojamäe, Hermansson, Dovesi *et al.*, 1994) and urea (Dovesi *et al.*, 1990), and which are known to underestimate experimental estimates based on sublimation enthalpies.

For each system in Table 1, sets of unique *hkl* were generated within the limit $(\sin\theta/\lambda)_{max} = 1.0$ Å^{-1} (Le Page & Gabe, 1979). Static structure factors (*i.e.* devoid of thermal motion) for the *molecules* calculations were obtained in the manner described previously (Spackman & Byrom, 1996); for the *crystal* calculation, they were obtained directly from *CRYSTAL*95. Although dynamic structure factors for *molecules* data can be obtained readily and have been described previously (Spackman & Byrom, 1996), for *crystal* data, the inclusion of thermal motion is not so straightforward. Approximate dynamic structure factors based on *CRYSTAL*95 results have been reported very recently by Lichanot and coworkers for silicon, MgO and BeO (Azavant *et al.*, 1994), MgF_2 (Azavant *et al.*, 1996) and cubic BN (Lichanot *et al.*, 1995), but there appear to have been no applications to molecular crystals. To approximate the effects of thermal motion in our study, the two data sets (*molecules* and *crystal*) generated for each molecular crystal were used as the 'observed' structure factors in least-squares refinements using *VALRAY* (Stewart & Spackman, 1983), with two different weighting schemes: (*a*) unit weights for all structure factors (labelled *static*); and (*b*) each structure factor weighted by $\exp[-2B(\sin\theta/\lambda)^2]$ (labelled *dynamic*).

The latter weighting scheme is equivalent to using an overall isotropic temperature factor of B for the 'observed' and fitted structure factors and, as demonstrated by Spackman & Byrom (1996), the results of such a refinement on *molecules* data closely mimic those obtained with anisotropic temperature factors. For this work, we use $B = 2.0$ Å^2 for all *dynamic* refinements, a value in line with reported thermal parameters for ice VIII, formamide and urea, and somewhat less than those for acetylene. All refinements were based on $|\Delta F|$, with fixed positional parameters and thermal motion parameters fixed at zero. As before, three multipole models were refined: *A*, monopoles only; *B*, multipole model with fixed exponents; and *C*, multipole model with optimized exponents. The nature of each is summarized

in Fig. 1; additional details have been provided previously.

3. The interaction density

Contour maps of the interaction density, $\rho_{\text{int}} = \rho_{\text{crystal}} - \sum\rho_{\text{molecule}}$, are plotted in Fig. 2 (at infinite resolution) and Fig. 3 (at the resolution of the model data sets, $\sin\theta/\lambda = 1.0$ Å^{-1}). The blurring of features with reducing resolution is important, and illustrative of the diminished information about sharp deformations available in an experimental electron distribution. Relevant to this study are the systematic polarization features due to hydrogen bonding in ice VIII, urea and formamide – a shift of electron density away from the H atoms involved in the hydrogen bond (making them more electropositive), and build-up between atoms in the O—H or N—H bonds. This feature is more exaggerated in the case of ice VIII than urea or formamide. The interaction density for ice VIII in Fig. 2 is in excellent agreement with those reported recently by Ojamäe, Hermansson, Dovesi *et al.* (1994) for three different pressures. As expected, acetylene shows very little interaction density, especially at the Hartree–Fock level, and conveniently serves as a control system (*i.e.* a molecular crystal exhibiting very small or negligible effects of intermolecular interaction) in our study.

The magnitude of the interaction densities in Figs. 2 and 3 is reflected in R factors ($\%R_F$) summarizing the agreement between the set of *crystal* and *molecules* static structure factors: ice VIII, 0.86%; acetylene, 0.13%; formamide, 0.65%; and urea, 0.39%. These figures represent rather important benchmarks in our later discussion on R factors for multipole fits to the *crystal* and *molecules* data sets.

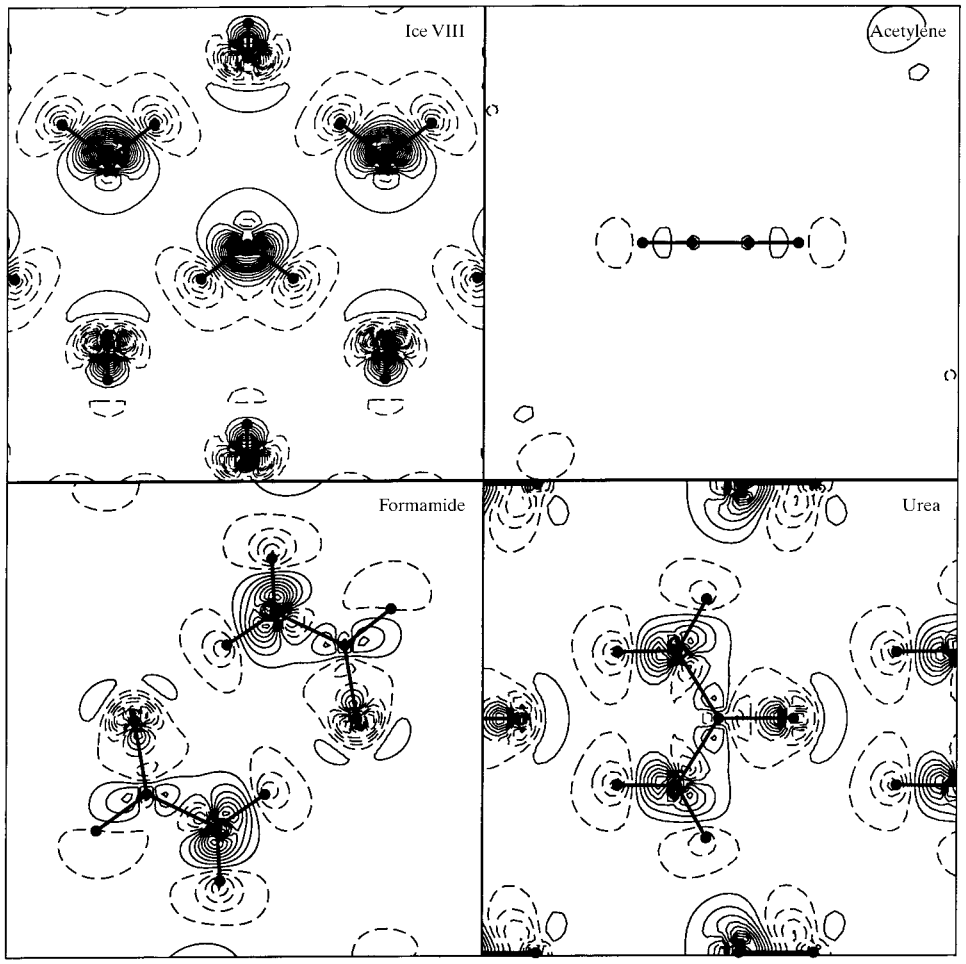

Fig. 2. Interaction density, ρ_{int}, the difference between the *ab initio* electron distributions for the crystal and a superposition of molecules in the lattice (see text) for the four molecular crystals studied. Contours at 0.025 e Å^{-3} intervals, zero contour omitted. The mapping planes are identical to those used in Figs. 3, 8 and 9.

4. Multipole fitting of model data sets

Our results will be examined under several headings. The first section discusses the quality of the fit obtained to the simulated diffraction data by examining two residuals. Then the values of the radial function exponents derived from the refinement will be investigated. Finally, we will discuss in some detail the representation of the interaction density with the two multipole models, *B* and *C*.

4.1. *Residuals and goodness of fit*

Tables 2 and 3 give final residuals, R_F, and goodness of fit, *S*, for static and dynamic refinements to both *crystal* and *molecules* data. The static *molecules* results for acetylene, formamide and urea are essentially those reported previously (Spackman & Byrom, 1996) (any differences reflect small changes in fractional coordinates or cell parameters). In addition to the conclusions reached earlier, we see here that, for hydrogen-bonded systems, models *B* and *C* generally fit the *crystal* data better than the *molecules* data; for acetylene, the reverse is marginally apparent. This is a curious result, but not, we believe, of much significance.

It is important to compare the values of $\%R_F$ in Table 2 with the indices given above for agreement between *molecules* and *crystal* data. For all systems, it is apparent that the effect of intermolecular interactions is of the same magnitude as the shortcomings of the multipole models, even where higher multipole exponents are refined (model *C*). Thus, for ice VIII, the best fit to either set of (static) data is 0.44%, roughly half the size of the effect of the interaction density (0.86%); for acetylene, the best fit is 0.54%, several times the size of the interaction density effect (0.13%); for formamide and urea, the best fits to static data are approximately the same size as the effect of intermolecular interactions. These results would seem to preclude any possibility

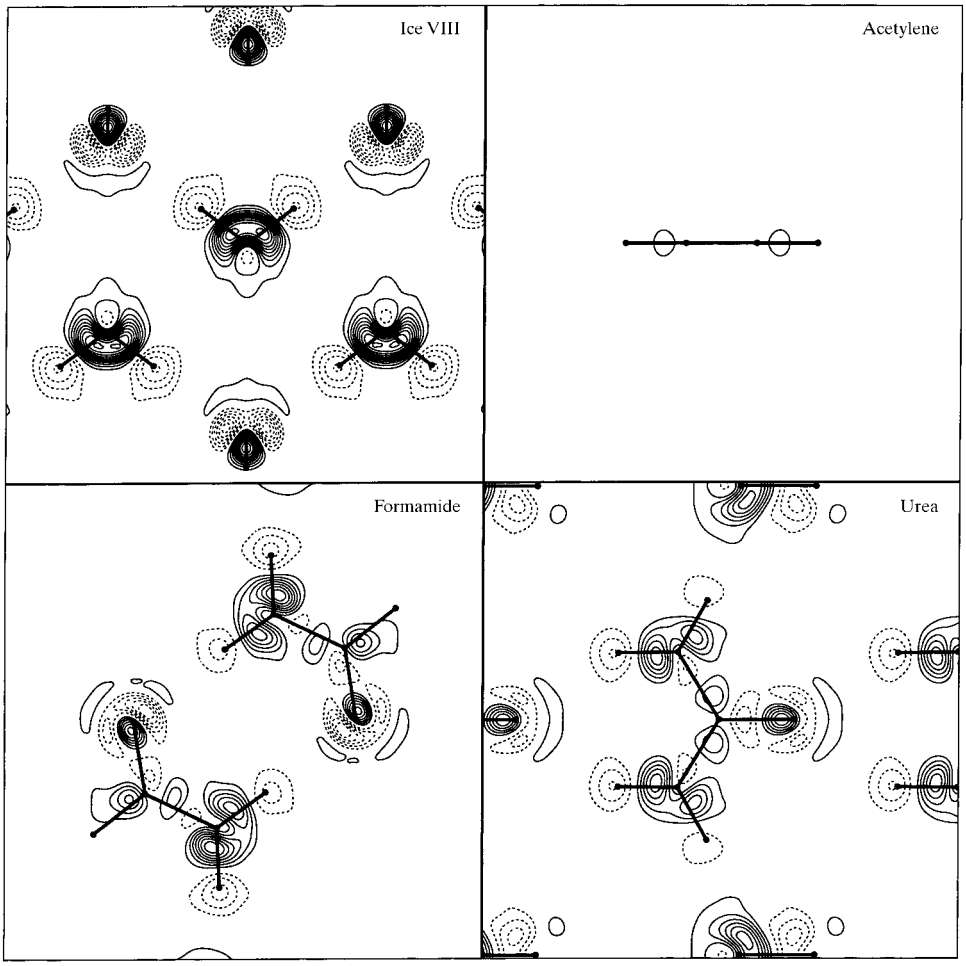

Fig. 3. Interaction density, $\rho_{\rm int}$, at a resolution of $\sin\theta/\lambda = 1.0$ Å^{-1}, obtained by Fourier summation of appropriately phased structure factors computed from the electron densities used in Fig. 2. Each map is 8 Å square, and atoms and bonds in, or projected onto, the planes are indicated; contours as in Fig. 2.

Table 2. *Percentage residuals,* $\%R_F = 100 \times \sum ||F_{obs}| - |F_{calc}|| / \sum |F_{obs}|$, *after multipole refinements (static and 'dynamic' – see text) with models A, B and C against crystal and molecules data*

The number of refined parameters, N_{param}, is given for each of models *A*, *B* and *C*, respectively, and is the same for fits to both static and dynamic data for the same system.

	Ice VIII		Acetylene		Formamide		Urea	
	Molecules	*Crystal*	*Molecules*	*Crystal*	*Molecules*	*Crystal*	*Molecules*	*Crystal*
	N_{param} = 5, 15, 17		N_{param} = 5, 12, 14		N_{param} = 11, 80, 84		N_{param} = 10, 39, 43	
Static refinement								
A	2.77	2.34	2.60	2.65	2.66	2.50	1.89	1.84
B	0.54	0.45	0.94	0.95	0.88	0.79	0.60	0.55
C	0.47	0.44	0.54	0.55	0.55	0.52	0.35	0.37
'Dynamic' refinement								
A	2.76	2.35	3.27	3.32	2.91	2.80	2.06	2.07
B	0.67	0.51	1.02	1.02	0.97	0.88	0.64	0.59
C	0.61	0.55	0.60	0.61	0.63	0.59	0.41	0.42

Table 3. *Goodness of fit,* $S = [\sum w(|F_{obs}| - |F_{calc}|)^2/(N_{obs} - N_{param})]^{1/2}$, *after multipole refinements (static and 'dynamic' – see text) with models A, B and C against crystal and molecules data*

The number of refined parameters, N_{param}, is given for each of models *A*, *B* and *C*, respectively, and is the same for fits to both static and dynamic data for the same system (N_{obs} is given in Table 1).

	Ice VIII		Acetylene		Formamide		Urea	
	Molecules	*Crystal*	*Molecules*	*Crystal*	*Molecules*	*Crystal*	*Molecules*	*Crystal*
	N_{param} = 5, 15, 17		N_{param} = 5, 12, 14		N_{param} = 11, 80, 84		N_{param} = 10, 39, 43	
Static refinement								
A	0.256	0.220	0.187	0.189	0.196	0.192	0.137	0.133
B	0.049	0.042	0.044	0.044	0.055	0.049	0.035	0.033
C	0.043	0.040	0.025	0.025	0.035	0.033	0.022	0.022
'Dynamic' refinement								
A	0.131	0.117	0.129	0.130	0.115	0.116	0.080	0.079
B	0.024	0.022	0.016	0.016	0.025	0.023	0.017	0.016
C	0.021	0.018	0.010	0.010	0.015	0.015	0.010	0.010

that models *B* and *C* are capable of fitting the interaction density with any accuracy whatsoever. However, we show below that this is not the case.

4.2. *Radial exponents and net charges*

Mean values of refined exponents for higher multipole functions are listed separately in Table 4 for fits to *molecules* and *crystal* data. For refinements against *molecules* data, the refined exponents differ little from those reported earlier (deduced from a larger sample of systems); our focus here is on the differences between fits to *molecules* and *crystal* – the effects of intermolecular interaction. We see a negligible difference for H and C atoms, but a noticeable difference for N and O atoms. The standard deviations reported in Table 4 pertain to the observed distribution of exponents, and actually obscure the systematic nature of the difference. In fact, for all N and O atoms in our study, and for both static and dynamic refinements, hydrogen bonding is always observed to reduce the refined exponent; mean decreases are (in a.u.) −0.15 (8) for nitrogen and −0.30 (8) for oxygen. We note with interest that the hydrogen bond evidently requires a subtly different description of the deformation electron density around the donor and acceptor heavy atoms (N and O in these examples) but not of the hydrogen atom participating in the bond. Along with the results obtained previously, we can now rather confidently suggest that the best exponent for a set of single radial functions for carbon atoms should be as much as 0.7 a.u. below the standard molecular (SM) result (Hehre *et al.*, 1969, 1970), that for nitrogen atoms should also be a little below the SM value (as much as 0.3 a.u. less), while the SM value should suffice for oxygen in a hydrogen-bonded environment.

Net atomic charges from multipole models are notoriously variable, and often exhibit counter-intuitive values. In the present study, this variability is evidenced in quite different results from models *B* and *C*, for

example for the carbon atom in formamide (*crystal*, static) model *B* yields a charge of +0.15 (2), while model *C* gives a charge of −0.20 (2). Nevertheless, for the hydrogen-bonded systems all models display a consistent trend in going from *molecules* results to *crystal* results, whereby the hydrogen atoms involved in the hydrogen bond become more positively charged (typically by less than 0.1 e), consistent with an enhancement of the dipole moment (see below). For urea and formamide, a direct comparison can be made with a result reported for urea by Gatti *et al.* (1994). Based on a topological analysis, that work reported a net flux of 0.067 e from the amino-group hydrogen donor to the carbonyl acceptor; for the urea (static) refinement in the present work, we obtain values of 0.046 (52) e (model *B*) and 0.074 (53) e (model *C*), and for the formamide (static) refinement we obtain fluxes of 0.064 (42) e (model *B*) and 0.082 (41) e (model *C*). Clearly, despite their lack of merit in absolute terms, net atomic charges from multipole refinements reflect the subtle effects of hydrogen bonding, although, because of the relatively small charge transfers involved and large standard error estimates, they are not likely to be useful diagnostic tools in population analysis.

4.3. *Retrieval of the interaction density*

As discussed above, simple inspection of *R* factors in Table 2 would suggest that multipole models incorporating higher angular functions (*B* and *C*) cannot

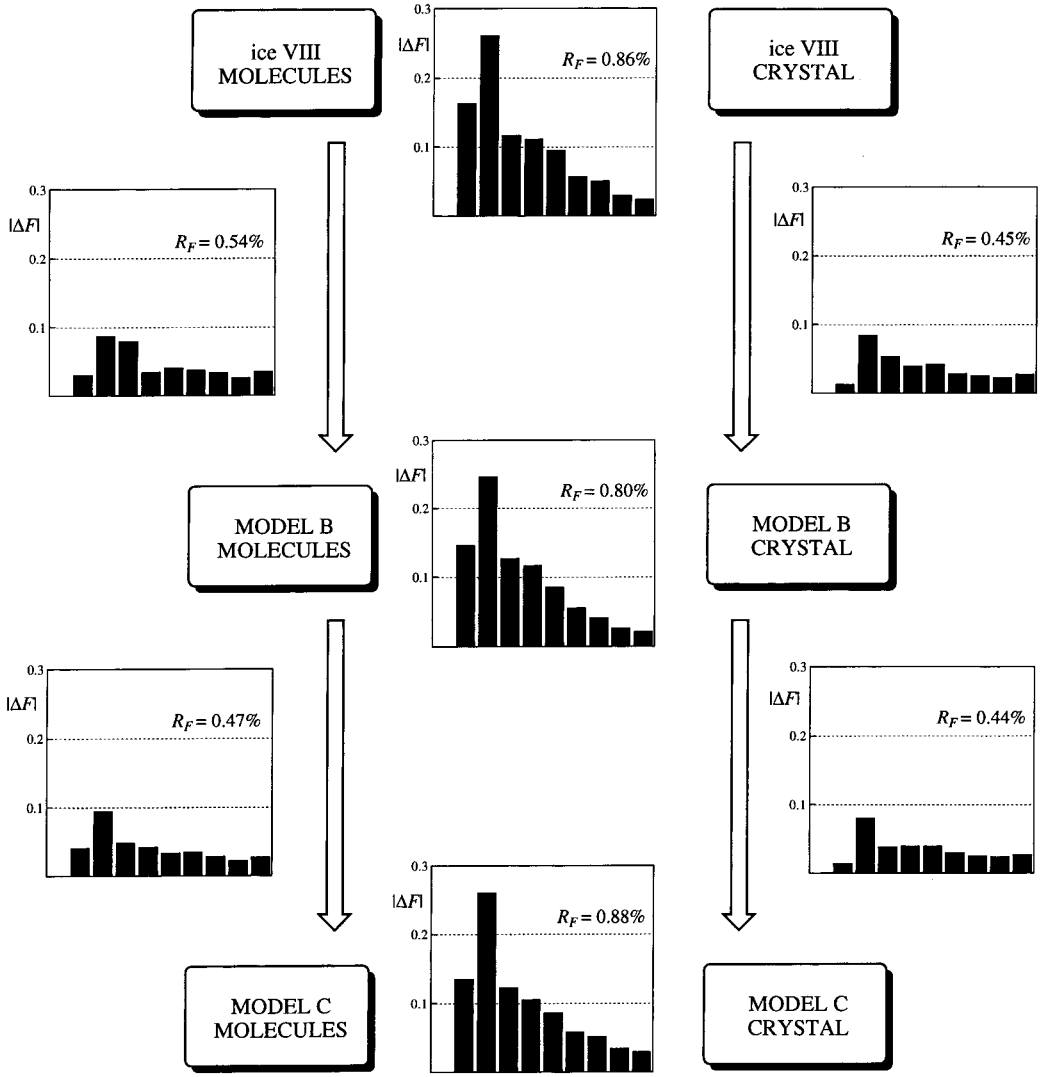

Fig. 4. Histograms summarizing structure-factor residuals for ice VIII after multipole refinements applied to static *molecules* and *crystal* data, as well as differences between the outcomes of the various models. Each histogram plots the mean values of $|\Delta F|$ over intervals of 0.10 Å^{-1}. Plots on the left and right reflect deficiencies of the multipole model, while those in the centre reflect the interaction density and its retrieval by multipole models *B* and *C*.

adequately describe the interaction density. To explore this notion further, we have constructed graphical summaries of the fitting procedure for models *B* and *C* refined against static *molecules* and *crystal* data for all four systems (Figs. 4–7). In these figures, we present fits to *molecules* data on the left, and fits to *crystal* data on the right. Differences between various models and datasets are displayed as *R* factors along with a spectral analysis of the residuals, the latter obtained by grouping reflections into intervals of 0.10 Å^{-1} in $\sin\theta/\lambda$, and for each interval graphing the mean absolute value of the differences in structure-factor magnitudes, labelled $|\Delta F|$ in the figures. A similar strategy was used by De Vries (1996) to discuss differences between data sets, but in that case individual *R* factors were reported for each data interval. We prefer to use $|\Delta F|$, which is a direct measure of the difference between structure-factor magnitudes. The histograms in Figs. 4–7 are therefore 'fingerprints' of either a shortcoming of the multipole model (*i.e.* the residual density; on the left and right of the figures) or the effect of intermolecular interactions (*i.e.* the interaction density; in the centre of each figure).

Bearing these points in mind, the figures highlight the following:

(*a*) The effect of intermolecular interactions is clearly largest for ice VIII (several tenths of an electron) and smallest for acetylene (typically much less that 0.05 e), in line with *R* factors listed above.

(*b*) In reciprocal space, the interaction density appears to peak near 0.2 Å^{-1}, and decays monotonically thereafter. With the possible exception of ice VIII (which is unusual – see above), there seems to be little information on the interactions beyond the resolution of these model datasets.

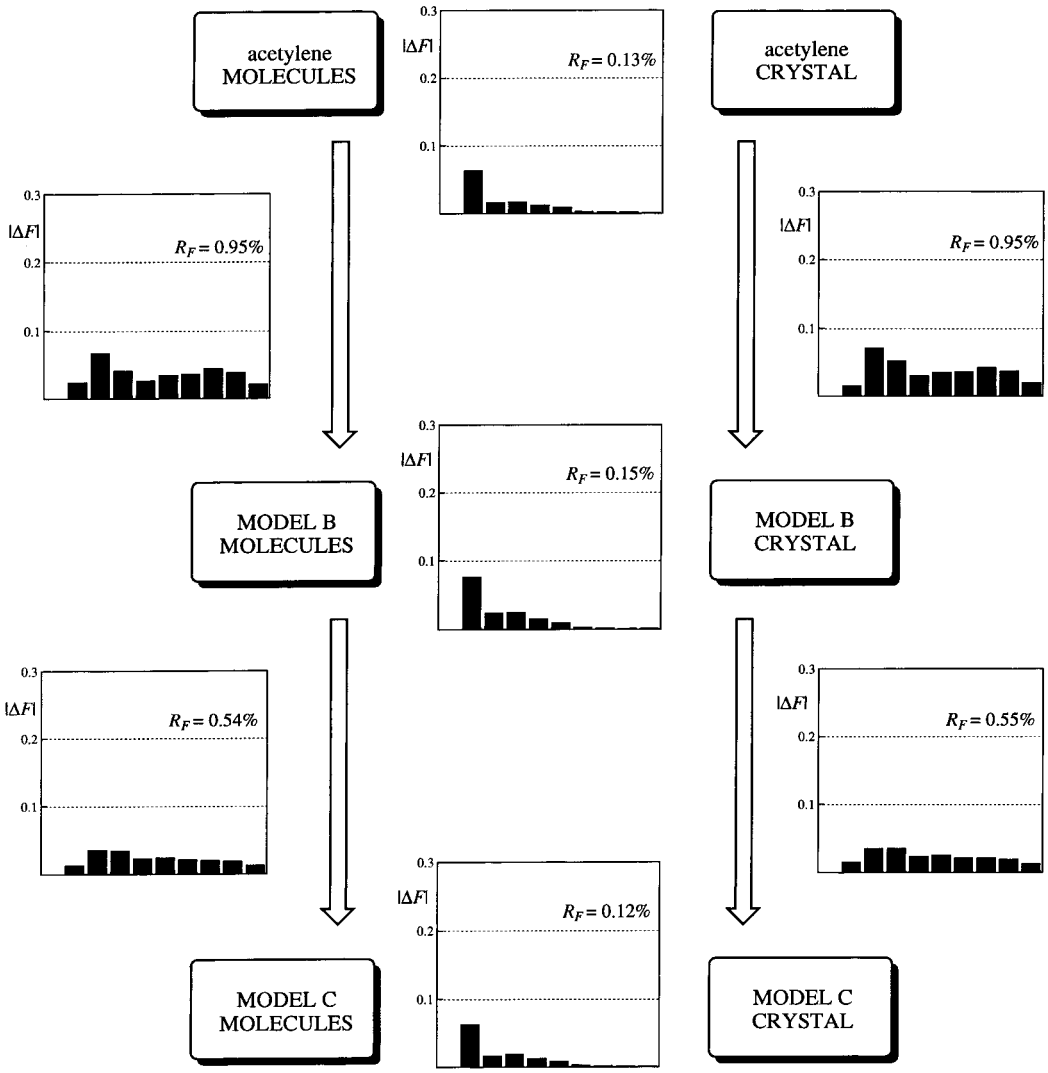

Fig. 5. Histograms as in Fig. 4 for acetylene.

Table 4. *Mean values of the refined exponents (in a.u.) for single exponential radial functions for each atom, compared with the standard molecular (Hehre et al., 1969, 1970) and single-zeta atomic values (Clementi & Roetti, 1974)*

Values listed are means over static and dynamic refinements for the four systems, with the standard deviation of the distribution in parentheses. For H, results are given separately for monopole functions.

Atom			*Molecules*		*Crystal*	Standard molecular	Atomic single-zeta
H	Monopole	*A*	2.72 (22)	*A*	2.74 (24)		
		B	2.26 (8)	*B*	2.28 (7)		
		C	2.29 (9)	*C*	2.32 (11)		
	Higher multipole		2.63 (14)		2.62 (11)	2.48	2.00
C			2.73 (11)		2.75 (10)	3.44	3.18
N			3.74 (17)		3.59 (12)	3.90	3.84
O			4.79 (26)		4.50 (31)	4.50	4.47

(*c*) The residual density also peaks at low $\sin\theta/\lambda$, but it does not decay monotonically or rapidly. It is quite clear that a substantial discrepancy remains between the model and the data beyond the resolution of the data.

(*d*) Both multipole models *B* and *C* appear to retrieve faithfully the fingerprint of the intermolecular interactions in all systems, with model *C* providing a marginally better result. This outcome is despite the often larger *R* factor describing the fit of the model to the *molecules* or *crystal* data.

For each of the four systems, Fourier maps of static interaction densities from models *B* and *C* are virtually identical with one another and, at the level of reproduction on the journal page, indistinguishable from those in Fig. 2. For comparison, we provide static residual density maps from models *B* (Fig. 8) and *C* (Fig. 9). Even allowing for the different contour intervals in the two sets of figures, there is little doubt that the multipole models are deficient in their description of the C—N, C═O and C═C bonds (especially in model *B*, where the radial exponent on carbon atoms is too large), whereas a dominant part of the interaction density is localized near the O—H and N—H bonds. We are led to the inescapable conclusion that both multipole models *B* and *C* retrieve almost all of the interaction density for these systems, despite substantial deficiencies of the models. In effect, the residual density would seem to be almost orthogonal to the interaction density.

4.4. *Induced dipole moment*

Molecular dipole moments have been obtained from the parameters in the multipole refinements by integration over the monopole and dipole functions belonging to a single molecule, and Table 5 summarizes the results for the three dipolar (hydrogen-bonded) systems. For fits to the *molecules* data, we have the isolated molecule value (*i.e.* target value from the *ab initio* calculation) available as a benchmark. As concluded previously (Spackman & Byrom, 1996), the monopole-only model (*A*) yields large errors and is generally inadequate at retrieving known dipole moments, while models *B* and *C* typically underestimate the known value, often by an unpredictable amount. In addition, fits to dynamic data (in this case refinements weighted to approximate such a fit) generally yield much improved estimates of dipole moments where these are known (and, by inference, where they are not known, such as in the crystal).

As discussed in the *Introduction*, a primary objective of the present paper is to examine the effect of intermolecular interactions on molecular moments derived from multipole refinements. From Table 5, we see that all models suggest a systematic enhancement of the dipole moment upon hydrogen bonding, although model *A* provides enhancements which are substantially lower than those from models *B* or *C*. The table reports mean enhancements, obtained from an average over the static and dynamic results for models *B* and *C*, along with a standard error in the distribution (of four values). For each system, the induced dipole moments from models *B* and *C*, whether from static or dynamic refinements, are remarkably constant, in spite of the considerable errors (both systematic and least squares in origin) associated with individual results in the table.

For ice VIII, our result of 0.58 (3) D compares favourably with 0.451 D reported by Gatti *et al.* (1995) from a topological partitioning of a periodic Hartree–Fock electron distribution for ice VIII. Other estimates of induced dipole moments in ices and liquid water range from 0.60 to 1.00 D (Coulson & Eisenberg, 1966; Barnes *et al.*, 1979; Cummins *et al.*, 1987; Sprik, 1991; Dang, 1992; Laasonen *et al.*, 1993; Bernardo *et al.*, 1994; Gregory *et al.*, 1997). The earliest of these estimates, that of Coulson & Eisenberg (1966) of 0.82 D, is frequently cited as an 'experimental estimate' in the recent literature, although it is nothing of the sort, being a calculation of the electric field arising from neighbouring molecules and the subsequent induced moment computed from known properties of the water molecule. Using a similar strategy, enhancements of 0.91 D (for an ice I_h cluster) and 0.85 (for a cyclic hexamer) have been obtained recently by Gregory *et al.* (1997), and these are

in accord with their *ab initio* calculations and spectroscopic observations on small water clusters. Other experimental estimates of molecular dipole moments for water molecules in various hydrates have been summarized by Spackman (1992), and exhibit a mean near 2.4 D with a standard deviation in the distribution of more than 0.4 D, the large spread reflecting the variety of multipole refinements used, the range of quality of the X-ray data sets, the differing environments of the water molecules, and the ambiguity in defining a molecule in a crystal. A more recent estimate of 2.1 D has been provided for a water molecule in ice I_h (van Beek *et al.*, 1996), although no error estimate was provided, and the inherently disordered nature of the ice I_h structure necessitated a number of assumptions in the derivation of this quantity.

For formamide, our estimate of the induced dipole moment is 1.32 (6) D, somewhat lower than the value of 1.98 D obtained from a topological partitioning of a periodic Hartree–Fock electron distribution (Gatti, 1996). Experimental estimates of the molecular dipole moment for formamide in the crystal have been reported from monopole and multipole refinement procedures [see Moss & Coppens (1980) and references therein]. The multipole refinement result of 4.83 D (likely to be an underestimate for the reasons discussed above) implies an induced dipole moment of 1.1 D.

In the case of urea, the present estimate of the induced dipole moment is 1.41 (6) D, also somewhat lower than the value (1.90 D) obtained from a topological partitioning of a periodic Hartree–Fock electron distribution (Gatti *et al.*, 1994). However, both of these theoretical results are consistent with an induced dipole moment of 1.6 (5) D implied by the multipole-derived estimate of the dipole moment in the crystal [5.4 (5) D] reported by Spackman *et al.* (1988).

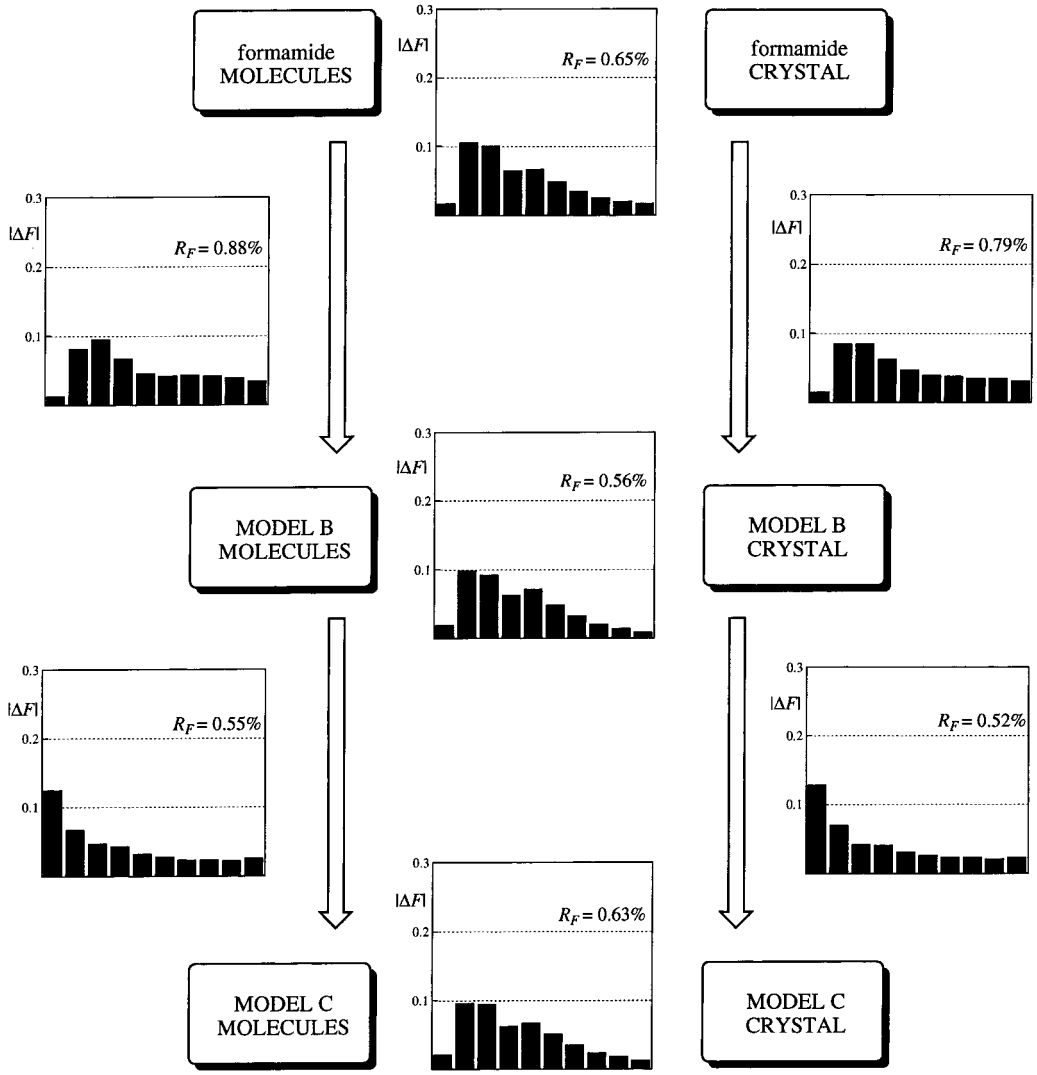

Fig. 6. Histograms as in Fig. 4 for formamide.

Table 5. *Estimated molecular dipole moments (D), and enhancements due to intermolecular interactions*

	Ice VIII		Formamide		Urea	
	Molecules	*Crystal*	*Molecules*	*Crystal*	*Molecules*	*Crystal*
Static refinement						
A	2.11 (29)	2.38 (25)	1.75 (38)	2.35 (37)	4.44 (63)	5.37 (61)
B	1.64 (11)	2.21 (9)	3.66 (14)	4.90 (12)	4.38 (26)	5.71 (24)
C	1.38 (10)	1.95 (10)	3.71 (11)	5.06 (10)	4.36 (18)	5.80 (19)
'Dynamic' refinement						
A	2.26 (20)	2.56 (18)	2.98 (25)	3.67 (25)	5.60 (42)	6.61 (40)
B	1.81 (8)	2.38 (7)	3.95 (8)	5.25 (7)	4.66 (16)	6.05 (15)
C	1.34 (8)	1.96 (8)	3.93 (6)	5.32 (6)	4.73 (11)	6.21 (11)
Isolated molecule (target) value	2.21		4.67		5.27	
Mean enhancement of dipole moment†	0.58 (3)		1.32 (6)		1.41 (6)	

† Dipole-moment enhancement is computed as a mean of both static and dynamic differences (*crystal* minus *molecules*) for models *B* and *C* only; figures in parentheses are standard errors in the distribution of results.

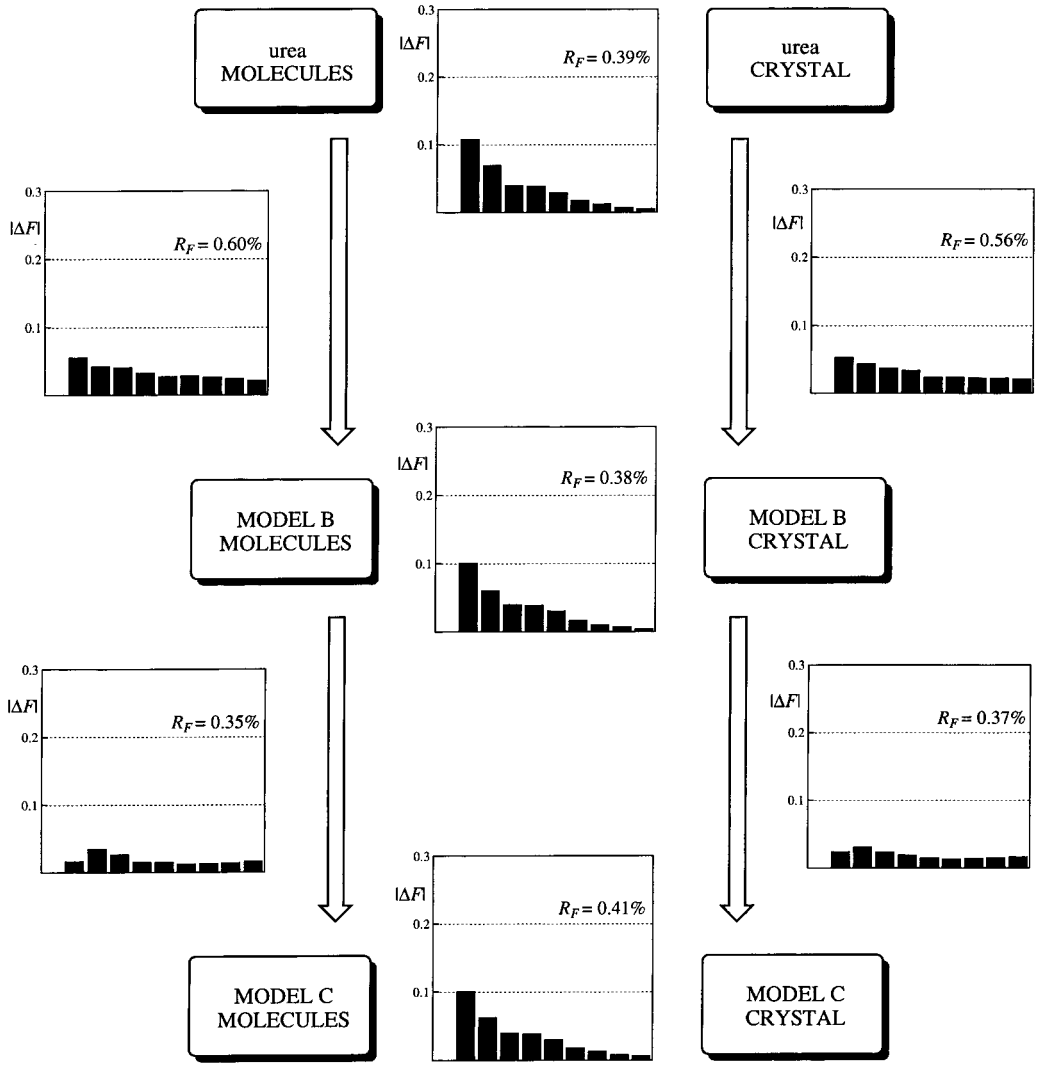

Fig. 7. Histograms as in Fig. 4 for urea.

Table 6. *Trace of the molecular second moment tensor, $\langle r^2 \rangle$ (e Å^2), estimated from multipole refinements*

Standard least-squares errors are in parentheses.

	Ice VIII		Acetylene		Formamide		Urea	
	Molecules	*Crystal*	*Molecules*	*Crystal*	*Molecules*	*Crystal*	*Molecules*	*Crystal*
Static refinement								
A	−3.89 (15)	−3.85 (13)	−8.30 (29)	−8.27 (29)	−12.21 (19)	−12.16 (19)	−14.44 (38)	−14.29 (36)
B	−3.77 (8)	−3.52 (7)	−7.36 (9)	−7.25 (9)	−10.98 (8)	−10.60 (7)	−14.01 (21)	−13.50 (20)
C	−3.98 (8)	−3.73 (8)	−6.85 (12)	−6.80 (12)	−10.80 (7)	−10.43 (6)	−13.63 (17)	−13.12 (18)
'Dynamic' refinement								
A	−3.78 (11)	−3.72 (9)	−7.54 (24)	−7.50 (24)	−11.44 (13)	−11.37 (13)	−13.61 (25)	−13.44 (24)
B	−3.58 (6)	−3.37 (5)	−7.23 (4)	−7.13 (4)	−10.81 (5)	−10.50 (4)	−13.73 (13)	−13.31 (12)
C	−3.99 (7)	−3.75 (6)	−7.15 (6)	−7.07 (6)	−10.81 (4)	−10.50 (4)	−13.46 (11)	−13.06 (11)
Isolated molecule (target) value	−3.59		−7.08		−10.66		−13.73	

4.5. *Second and quadrupole moments*

Table 6 summarizes results for the trace of the molecular second-moment tensors, which support the conclusions of previous work (Spackman & Byrom, 1996). The effect of intermolecular interactions is observed to be small, with a systematic (albeit marginally significant) reduction in $\langle r^2 \rangle$ perceptible, especially for urea and formamide. Unfortunately, no comparable results from theoretical calculations appear to have been published.

Here we wish to focus in some detail on both second moments and quadrupole moments, and restrict the discussion to results obtained for just acetylene and urea (Table 7); for formamide, the lower symmetry complicates the discussion. For the purposes of discussion, we recall that the second moments are simple expectation values of the total charge density, for example:

$$\mu_{xy} = \int_V \rho(\mathbf{r})\, xy \, \mathrm{d}\mathbf{r},$$

with similar expressions for the other moments [here $\rho(\mathbf{r})$ includes both the negative electron density and positive nuclei, and the integration is over all space, but only for the multipole functions belonging to a single molecule removed from the crystal]. Quadrupole moments are readily derived from the second moments (but not *vice versa*):

$$\theta_{xx} = \mu_{xx} - (1/2)(\mu_{yy} + \mu_{zz}),$$
$$\theta_{xy} = (3/2)\mu_{xy},$$

with cyclic permutations of x, y and z yielding the other components. We note that diagonal elements of the second-moment tensor allow a direct interpretation of the effects of intermolecular interaction: an increase in magnitude (*i.e.* a more negative value) arises from an expansion of the electron density along that direction. Quadrupole moments mix the second moments and obscure this simple interpretation.

We discuss the *molecules* results first. As far as comparison with target results (given in Table 7 on the far right) for *molecules* data, dynamic refinements generally provide better results than their static counterpart, in agreement with previous observations (Spackman & Byrom, 1996). Models *B* and *C* yield results in quantitative agreement with target values, while results for model *A* are markedly inferior, and accompanied with larger least-squares uncertainties. Much of the poor performance of the monopoles-only model can be traced to the fact that the in-plane (μ_{xx} and μ_{zz} for urea) and parallel (μ_{zz} for acetylene) components are relatively poorly determined, exhibiting large least-squares errors, while the out-of-plane (μ_{yy} for urea) and perpendicular (μ_{xx} for acetylene) components are rather well determined. This behaviour reflects the differing contributions of the model to the perpendicular (out-of-plane) moments (only expansion/contraction of the pseudoatoms and atomic quadrupoles), whereas the parallel (in-plane) moments contain contributions from expansion/contraction, net atomic charges, as well as atomic dipoles and quadrupoles.

To see the effects of intermolecular interaction, we must focus on either both columns of static results, or both columns of dynamic results in Table 7. For acetylene, we observe a small contraction of the electron cloud along the molecular axis (μ_{zz}), with negligible change perpendicular to this axis, while for urea there is negligible change perpendicular to the molecular plane (μ_{yy}), a large contraction in the plane and perpendicular to the twofold axis (μ_{xx}), and a small contraction along the twofold axis (μ_{zz}). Interestingly, for urea these trends are in complete agreement with those observed by Spackman (1992), on the basis of analyses of experimental data, although the magnitude of the differences is roughly one-half to one-third those predicted earlier. We conclude that second moments extracted from diffraction data are likely to be close to those for isolated molecules, even for hydrogen-bonded systems, and the effects of intermolecular interactions

will be implicit in the results, but of limited significance even with error-free data. Quadrupole moments will be much less useful, amplifying small deficiencies in the present multipole model.

4.6. *Electric field gradients (EFGs)*

To simplify discussion of EFGs, we present and analyse only the largest principal component of the EFG tensor, conventionally labelled ∇E_{33}, for each atom, omitting discussion of the orientation of the EFG tensor in the crystal as well as its anisotropy, η, both of which are required for a detailed discussion of EFGs. Essentially, we focus on the most important quantity, related as it is to the nuclear quadrupole coupling constant (NQCC) observed experimentally. Our interest is in the retrieval of known quantities (obtained from *ab initio* molecular or crystal wavefunctions) as well as the effect of the crystal environment on the property. Only results obtained with multipole models *B* and *C* will be discussed, and these are reported in Table 8, along with relevant *ab initio* results.

Before discussing our multipole refinement results, it is worthwhile gaining an appreciation of how realistic our *ab initio* numbers are, how they compare with other calculations and with experiment. We note that there is little sense in performing a detailed comparison with previous theoretical results, as different nuclear geometries can have a substantial effect on the computed values. In general terms, our present *ab initio* results agree well with those obtained previously for isolated molecules or the crystal with similar basis sets and at the self-consistent field (SCF) level [H_2O (Huber, 1985; Cummins *et al.*, 1987; Gerber & Huber, 1989; Eggenberger *et al.*, 1992; Palmer, 1996), acetylene (Huber, 1985; Gerber & Huber, 1989), formamide (Palmer, 1988, 1996; Palmer & Blair-Fish, 1994; Palmer & Sherwood, 1996), urea (Palmer & Blair-Fish, 1994; Palmer & Sherwood, 1996)], and generally underestimate experimental results, but most of this discre-

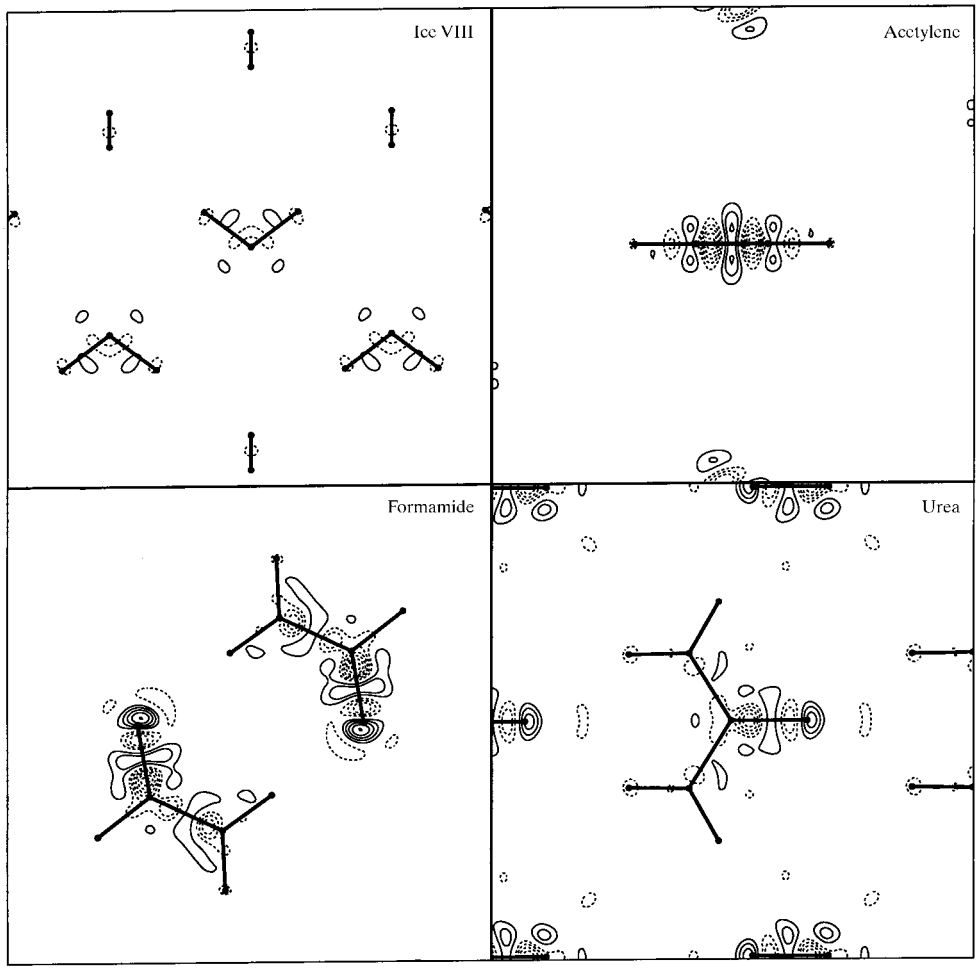

Fig. 8. Fourier maps ($\sin\theta/\lambda \leq 1.0$ Å^{-1}) of the static residual electron densities for model *B*, fitted to *molecules* data. Maps for fits to *crystal* data are virtually identical to these. Mapping planes as in Fig. 3, contours at 0.05 e Å^{-3} intervals, zero contour omitted.

Table 7. *Second and quadrupole moments (e Å^2) for acetylene and urea; standard least-squares errors are in parentheses*

A, *B* and *C* refer to results obtained with those multipole models. For acetylene, the molecular axis is the *z* axis, and, for urea, the molecule lies in the *xz* plane with *z* along the twofold axis.

		Molecules		*Crystal*		Isolated molecule (target) value
		Static	Dynamic	Static	Dynamic	
Acetylene						
μ_{xx}	*A*	−3.06 (6)	−2.88 (6)	−3.06 (6)	−2.88 (6)	−2.839
	B	−2.88 (2)	−2.85 (1)	−2.89 (2)	−2.86 (1)	
	C	−2.72 (3)	−2.82 (1)	−2.74 (3)	−2.83 (1)	
μ_{zz}	*A*	−2.19 (22)	−1.79 (17)	−2.14 (22)	−1.73 (17)	−1.401
	B	−1.60 (7)	−1.52 (3)	−1.48 (7)	−1.41 (3)	
	C	−1.41 (7)	−1.50 (3)	−1.32 (7)	−1.40 (4)	
θ_{zz}	*A*	0.87 (21)	1.09 (16)	0.92 (21)	1.15 (16)	1.438
	B	1.27 (7)	1.33 (3)	1.41 (7)	1.45 (3)	
	C	1.32 (6)	1.32 (3)	1.42 (6)	1.43 (3)	
Urea						
μ_{xx}	*A*	−3.84 (26)	−3.30 (17)	−3.70 (25)	−3.15 (16)	−3.277
	B	−3.46 (13)	−3.30 (8)	−3.15 (12)	−3.00 (8)	
	C	−3.45 (10)	−3.28 (7)	−3.08 (11)	−2.95 (6)	
μ_{yy}	*A*	−5.46 (5)	−5.32 (5)	−5.47 (5)	−5.33 (5)	−5.394
	B	−5.45 (4)	−5.40 (2)	−5.40 (4)	−5.36 (2)	
	C	−5.19 (4)	−5.22 (2)	−5.17 (4)	−5.21 (2)	
μ_{zz}	*A*	−5.14 (16)	−4.98 (10)	−5.11 (15)	−4.96 (10)	−5.056
	B	−5.09 (9)	−5.04 (5)	−4.95 (8)	−4.94 (5)	
	C	−4.98 (6)	−4.96 (4)	−4.86 (6)	−4.90 (4)	
θ_{xx}	*A*	1.46 (23)	1.85 (15)	1.59 (23)	2.00 (14)	1.948
	B	1.81 (12)	1.92 (7)	2.02 (11)	2.15 (7)	
	C	1.64 (8)	1.81 (5)	1.93 (8)	2.10 (5)	
θ_{yy}	*A*	−0.98 (7)	−1.18 (11)	−1.07 (16)	−1.27 (10)	−1.228
	B	−1.17 (8)	−1.23 (5)	−1.35 (7)	−1.38 (5)	
	C	−0.98 (6)	−1.10 (4)	−1.20 (6)	−1.28 (3)	
θ_{zz}	*A*	−0.49 (16)	−0.67 (11)	−0.52 (16)	−0.72 (10)	−0.721
	B	−0.64 (8)	−0.69 (5)	−0.67 (8)	−0.76 (5)	
	C	−0.66 (5)	−0.71 (3)	−0.74 (6)	−0.82 (3)	

pancy is removed with larger basis sets and electron correlation (Huber, 1985; Gerber & Huber, 1989; Palmer, 1996). Our *ab initio* results are discussed below for each system in turn.†

Ice VIII: The magnitude of ∇E_{33} for H is reduced by 0.39 e Å^{-3} upon hydrogen bonding in the crystal. This is somewhat less than the reduction of 0.72 e Å^{-3} implied by experimental results [isolated molecule, 3.09 (2) e Å^{-3} (Bluyssen *et al.*, 1967); ice VIII crystal, 2.37 (2) e Å^{-3} (Edmonds *et al.*, 1977)], no doubt in part because our *molecule* result refers to a nuclear geometry already distorted as in the crystal. For O the crystal environment reduces $|\nabla E_{33}|$ by 3.50 e Å^{-3}, in agreement with the experimentally observed effect [isolated molecule, 11.42 (18) e Å^{-3} (Verhoeven *et al.*, 1969); ice VIII crystal, 8.02 (18) e Å^{-3} (Edmonds *et al.*, 1977)].

† For comparison between experiment and theory, we have converted all experimental NQCCs to EFGs (in e Å^{-3}) using $(-\nabla E_{33}/\text{e Å}^{-3}) = 28.7206\ (\chi/\text{MHz})/(Q/\text{mb})$ (1 mb = 10^{-31} m^2) with Q(N) = 20.2 (3), Q(O) = −25.58 (22) and Q(D) = 2.860 (15) mb (Pyykkö & Li, 1992). The errors quoted here for experimental EFGs incorporate errors in both NQCC and Q.

Acetylene: ∇E_{33} for H is almost unaltered by the crystal environment, and much of the small change that does occur can be accounted for by molecular overlap rather than a specific interaction. Our numbers are unrealistic [*cf.* −1.99 (8) e Å^{-3} observed in nematic solution (Millett & Dailey, 1972) and −2.25 e Å^{-3} from an MP4 calculation (Gerber & Huber, 1989)] owing to our use of the atomic coordinates of McMullan *et al.* (1992) uncorrected for thermal motion. This will not compromise our multipole modelling of EFGs below.

Formamide: $|\nabla E_{33}|$ for both hydrogen atoms involved in hydrogen bonding (H2 and H3 in Table 8) is reduced by more than 0.3 e Å^{-3}, while for H1 (bonded to carbon) a much smaller decrease is evident. $|\nabla E_{33}|$ at N is reduced by 2.08 e Å^{-3}, in agreement with experiment [isolated molecule, 5.47 (8) e Å^{-3} (Kukolich & Nelson, 1971); undeuterated powder, 3.23 (6) e Å^{-3} (Hunt & Mackay, 1974)]. For O, our *ab initio* results suggest a reduction in $|\nabla E_{33}|$ by 2.17 e Å^{-3}.

Urea: Hydrogen bonding decreases $|\nabla E_{33}|$ at H atoms by as much as 0.25 e Å^{-3}, somewhat less than we calculate for formamide. The reduction at nitrogen,

1.46 e Å^{-3}, is also smaller than that computed for formamide, and in line with the theoretical result reported by Palmer & Blair-Fish (1994). An even smaller reduction, 0.86 e Å^{-3}, occurs at oxygen. Experimental NQCCs appear only to have been reported for the solid state, and only for ^{14}N (O'Konski & Torizuka, 1969) and ^{2}H (Chiba, 1965).

Although not experimentally relevant because no carbon isotopes have quadrupolar nuclei, it is interesting to observe that the computed effect of intermolecular interactions on ∇E_{33} at C nuclei is relatively small compared with the changes occurring at N and O. The change is typically between 0.2 and 0.5 e Å^{-3}, and in all cases represents an increase in magnitude, again contrary to the trend exhibited by N and O.

We now turn our attention to the retrieval of ∇E_{33}, both in absolute terms as well as the change brought about by intermolecular interactions, and note before discussing the results for each nucleus in turn that it is important to appreciate that the values in Table 8 have not all been obtained in the same manner. The *GAMESS* target value refers to integration over the *ab initio* electron density of an isolated molecule, the multipole refined results for both *molecules* and *crystal* have been obtained from integration over the multipole electron density functions belonging to a single molecule within the crystal. The *CRYSTAL* results, on the other hand, derive from integration over the *ab initio* crystalline electron distribution. We have compared *crystal* results obtained by summation over a single molecule and the lattice, and conclude that these simple overlap effects are of the order of 0.1 e Å^{-3}, depend on the local environment of the particular nuclei, and are greatest for atoms on the periphery of a molecule. We have not included them systematically here, but expect that they will be essential in future detailed analyses of EFGs extracted from diffraction data, especially for H atoms.

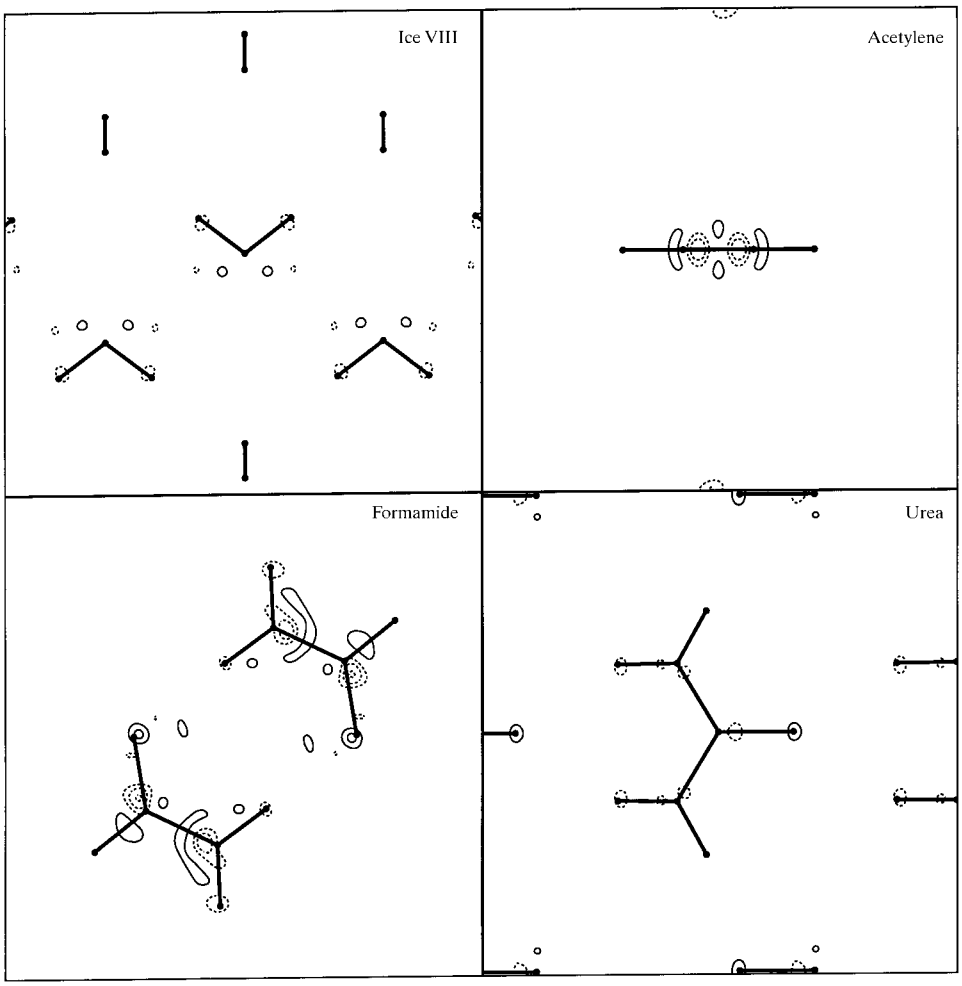

Fig. 9. Fourier maps ($\sin\theta/\lambda \leq 1.0$ Å^{-1}) of the static residual electron densities for model *C*, fitted to *molecules* data. Maps for fits to *crystal* data are virtually identical to these. Mapping planes as in Fig. 3, contours at 0.05 e Å^{-3} intervals, zero contour omitted.

Table 8. *Largest principal components of the EFG tensor, ∇E_{33} (e Å^{-3}), at each atomic nucleus*

For formamide, H3 is the hydrogen atom attached to carbon, H2 on nitrogen and *syn* to oxygen, H1 on nitrogen *anti* to oxygen, and for urea H1 is the hydrogen atom *syn* to oxygen, H2 *anti* to oxygen.

		Molecules		*GAMESS*	*Crystal*		*CRYSTAL*
		Model *B*	Model *C*	target value	Model *B*	Model C	target value
Ice VIII							
Static	O	8.67	9.57	13.23	6.51	6.60	9.73
	H	−3.20	−3.25	−3.23	−2.78	−2.87	−2.84
Dynamic	O	8.57	8.14		6.44	5.49	
	H	−3.06	−3.24		−2.67	−2.91	
Acetylene							
Static	C	3.27	2.20	1.40	3.33	2.32	1.60
	H	−3.35	−3.21	−3.17	−3.28	−3.16	−3.11
Dynamic	C	3.86	2.65		4.00	2.79	
	H	−3.28	−3.28		−3.23	−3.23	
Formamide							
Static	O	7.87	10.13	12.51	6.59	7.82	10.34
	N	3.92	3.91	6.81	2.35	2.10	4.73
	C	−4.83	−3.54	−3.71	−5.18	−3.90	−4.19
	H1	−3.07	−2.88	−2.98	−2.75	−2.61	−2.64
	H2	−2.96	−2.76	−2.88	−2.68	−2.53	−2.55
	H3	−2.03	−1.96	−2.03	−1.93	−1.84	−1.95
Dynamic	O	7.61	9.62		6.34	6.90	
	N	3.45	2.95		1.86	1.53	
	C	−5.39	−3.63		−5.66	−3.93	
	H1	−3.01	−2.95		−2.69	−2.66	
	H2	−2.87	−2.78		−2.61	−2.58	
	H3	−1.97	−1.93		−1.88	−1.82	
Urea							
Static	O	7.18	8.67	10.98	6.08	6.76	10.12
	N	4.51	4.70	7.89	3.46	3.48	6.43
	C	−5.17	−3.47	−3.35	−5.31	−3.68	−3.67
	H1	−3.03	−2.78	−2.87	−2.81	−2.63	−2.64
	H2	−3.07	−2.88	−3.02	−2.82	−2.66	−2.77
Dynamic	O	6.99	8.15		5.80	5.64	
	N	3.98	3.71		2.94	2.77	
	C	−5.67	−3.49		−5.72	−3.71	
	H1	−2.99	−2.86		−2.79	−2.70	
	H2	−3.05	−2.94		−2.79	−2.72	

EFGs computed from multipole models *B* and *C* (Table 8) fully support the conclusions obtained previously (Spackman & Byrom, 1996) regarding underestimation of $|\nabla E_{33}|$ for O and N, better performance for C, and excellent retrieval for H. In addition, we see that the effect of intermolecular interactions is typically underestimated at C, N and O nuclei, but retrieved quantitatively at H nuclei. The successful retrieval of EFGs at H nuclei applies for both static and dynamic data, and is noticeably better with the most flexible multipole model (*C*). Nevertheless, $|\nabla E_{33}|$ at H appears to be slightly underestimated, partly because of the use of a summation over a single molecule in the *crystal* case. Further more-detailed calibration of the retrieval of EFGs will need to be based upon the entire EFG tensor, including its direction in the crystal, and these studies will have to incorporate the effects of molecular overlap.

5. Final remarks

This study has addressed one limitation of a related earlier model study (Spackman & Byrom, 1996), namely the effect of including both weak and strong intermolecular interactions. To answer the questions raised in the *Introduction*:

(*a*) Hydrogen bonding manifests itself in localized depletions of electron density around H nuclei, with concomitant increases in the adjacent O—H and N—H bonds of the acceptor. More complex polarizations are evident at the acceptor atoms. Weak interactions, such as those in acetylene, have a negligible effect on the electron density. In reciprocal space, hydrogen bonding results in a significant (less than 1%) change in structure factors at low angles, decreasing quickly at higher angles; most of the effect is seen to occur for $\sin\theta/\lambda \leq 1.0$ Å^{-1}.

(*b*) We expect that the effects of intermolecular interactions will be measurable in careful experiments, but need to clarify this with careful model studies including random errors. Without random errors (noise), intermolecular interactions are seen to have an observable effect on the outcomes of multipole refinement procedures, especially dipole moments and EFGs, and it is quite clear that the interaction density can be retrieved quantitatively with a good multipole model, in spite of the increasingly evident inadequacies of radial functions in present multipole models (Chandler & Spackman, 1982; Moss *et al.*, 1995; Iversen *et al.*, 1997).

Work in progress addresses the incorporation of random noise and the extent to which this might modify these conclusions. We are also exploring multipole models which incorporate improved radial functions.

We are grateful to the Australian Research Council and the Swedish Natural Science Research Council (NFR) for support of this work.

References

Arnold, H. (1989). *International Tables for Crystallography*, Vol. A, *Space Group Symmetry*, edited by T. Hahn, pp. 69–79. Dordrecht: Kluwer Academic Publishers.

Azavant, P., Lichanot, A., Rerat, M. & Chaillet, M. (1994). *Theor. Chim. Acta*, **89**, 213–226.

Azavant, P., Lichanot, A., Rerat, M. & Pisani, C. (1996). *Int. J. Quantum Chem.* **58**, 419–429.

Bader, R. F. W. (1990). *Atoms in Molecules – a Quantum Theory*. Oxford University Press.

Barnes, P., Finney, J. L., Nicholas, J. D. & Quinn, J. E. (1979). *Nature (London)*, **282**, 459–464.

Beek, C. G. van, Overeem, J., Ruble, J. & Craven, B. M. (1996). *Can. J. Chem.* **74**, 943–950.

Bernardo, D. N., Ding, Y., Krogh-Jespersen, K. & Levy, R. M. (1994). *J. Phys. Chem.* **98**, 4180–4187.

Bluyssen, H., Verhoeven, J. & Dymanus, A. (1967). *Phys. Lett.* **25**A, 214–215.

Chandler, G. S. & Spackman, M. A. (1982). *Acta Cryst.* A**38**, 225–239.

Chiba, T. (1965). *Bull. Chem. Soc. Jpn*, **38**, 259–263.

Clementi, E. & Roetti, C. (1974). *At. Data Nucl. Data Tables*, **14**, 177–478.

Coppens, P., Dam, J., Harkema, S., Feil, D., Feld, R., Lehmann, M. S., Goddard, R., Krüger, C., Hellner, E., Johansen, H., Larsen, F. K., Koetzle, T. F., McMullan, R. K., Maslen, E. N. & Stevens, E. D. (1984). *Acta Cryst.* A**40**, 184–195.

Coulson, C. A. & Eisenberg, D. (1966). *Proc. R. Soc. London Ser. A*, **291**, 445–453.

Cummins, P. L., Bacskay, G. B. & Hush, N. S. (1987). *Mol. Phys.* **61**, 795–811.

Dang, L. X. (1992). *J. Chem. Phys.* **97**, 2659–2660.

De Vries, R. I. J. (1996). PhD thesis, University of Twente, Enschede, The Netherlands.

Dovesi, R., Causa, M., Orlando, R., Roetti, C. & Saunders, V. R. (1990). *J. Chem. Phys.* **92**, 7402–7411.

Dovesi, R., Saunders, V. R. & Roetti, C. (1992). *CRYSTAL92. An Ab Initio Hartree–Fock Program for Periodic Systems – User Documentation*. University of Turin, Italy.

Dovesi, R., Saunders, V. R., Roetti, C., Causa, M., Harrison, N. M., Orlando, R. & Apra, E. (1996). *CRYSTAL95 Users Manual*. University of Turin, Italy.

Edmonds, D. T., Goren, S. D., White, A. A. L. & Sherman, W. F. (1977). *J. Mag. Res.* **27**, 35–44.

Eggenberger, R., Gerber, S., Huber, H., Searles, D. & Welker, M. (1992). *J. Mol. Spectrosc.* **151**, 474–481.

Gatti, C. (1996). *Acta Cryst.* A**52**, C555.

Gatti, C., Saunders, V. R. & Roetti, C. (1994). *J. Chem. Phys.* **101**, 10686–10696.

Gatti, C., Silvi, B. & Colonna, F. (1995). *Chem. Phys. Lett.* **247**, 135–141.

Gerber, S. & Huber, H. (1989). *J. Mol. Spectrosc.* **134**, 168–175.

Gregory, J. G., Clary, D. C., Liu, K., Brown, M. G. & Saykally, R. J. (1997). *Science*, **275**, 814–817.

Hehre, W. J., Ditchfield, R., Stewart, R. F. & Pople, J. A. (1970). *J. Chem. Phys.* **52**, 2769–2773.

Hehre, W. J., Stewart, R. F. & Pople, J. A. (1969). *J. Chem. Phys.* **51**, 2657–2664.

Hermansson, K. (1985). *Acta Cryst.* B**41**, 161–169.

Hermansson, K. & Lunell, S. (1982). *Acta Cryst.* B**38**, 2563–2569.

Huber, H. (1985). *J. Chem. Phys.* **83**, 4591–4598.

Hunt, M. J. & Mackay, A. L. (1974). *J. Mag. Res.* **15**, 402–414.

Iversen, B. B., Larsen, F. K., Figgis, B. N. & Reynolds, P. A. (1997). *J. Chem. Soc. Dalton Trans.* pp. 2227–2240.

Krijn, M. P. C. M. & Feil, D. (1988*a*). *J. Chem. Phys.* **89**, 4199–4208.

Krijn, M. P. C. M. & Feil, D. (1988*b*). *J. Chem. Phys.* **89**, 5787–5793.

Krijn, M. P. C. M., Graafsma, H. & Feil, D. (1988). *Acta Cryst.* B**44**, 609–616.

Kuhs, W. F., Finney, J. L., Vettier, C. & Bliss, D. V. (1984). *J. Chem. Phys.* **81**, 3612–3623.

Kukolich, S. G. & Nelson, A. C. (1971). *Chem. Phys. Lett.* **11**, 383–384.

Laasonen, K., Sprik, M., Parrinello, M. & Car, R. (1993). *J. Chem. Phys.* **99**, 9080–9089.

Le Page, Y. & Gabe, E. J. (1979). *J. Appl. Cryst.* **12**, 464–466.

Lichanot, A., Rerat, M. & Catti, M. (1995). *Acta Cryst.* A**51**, 323–328.

McMullan, R. K., Kvick, Å. & Popelier, P. (1992). *Acta Cryst.* B**48**, 726–731.

Millett, F. S. & Dailey, B. P. (1972). *J. Chem. Phys.* **56**, 3249–3256.

Moss, G. & Coppens, P. (1980). *Chem. Phys. Lett.* **75**, 298–302.

Moss, G. R., Souhassou, M., Blessing, R. H., Espinosa, E. & Lecomte, C. (1995). *Acta Cryst.* B**51**, 650–660.

Ojamäe, L., Hermansson, K., Dovesi, R., Roetti, C. & Saunders, V. R. (1994). *J. Chem. Phys.* **100**, 2128–2138.

Ojamäe, L., Hermansson, K., Pisani, C., Causa, M. & Roetti, C. (1994). *Acta Cryst.* B**50**, 268–279.

O'Konski, C. T. & Torizuka, K. (1969). *J. Chem. Phys.* **51**, 461–463.

Palmer, M. H. (1988). *Chem. Phys.* **127**, 335–341.

Palmer, M. H. (1996). *Z. Naturforsch. Teil A*, **51**, 442–450.

Palmer, M. H. & Blair-Fish, J. A. (1994). *Z. Naturforsch. Teil A*, **49**, 146–154.

Palmer, M. H. & Sherwood, P. (1996). *Z. Naturforsch. Teil A*, **51**, 460–478.

Platts, J. A. & Howard, S. T. (1996). *J. Chem. Phys.* **105**, 4668–4674.

Pyykkö, P. & Li, J. (1992). *1992 Nuclear Quadrupole Moments*. Department of Chemistry, University of Helsinki, Finland.
Schmidt, M. W., Baldridge, K. K., Boatz, J. A., Elbert, S. T., Gordon, M. S., Jensen, J. H., Koseki, S., Matsunaga, N., Nguyen, K. A., Su, S., Windus, T. L., Dupuis, M. & Montgomery, J. A. (1993). *J. Comput. Chem.* **14**, 1347–1363.
Spackman, M. A. (1992). *Chem. Rev.* **92**, 1769–1797.
Spackman, M. A. & Byrom, P. G. (1996). *Acta Cryst.* B**52**, 1023–1035.
Spackman, M. A., Weber, H.-P. & Craven, B. M. (1988). *J. Am. Chem. Soc.* **110**, 775–782.
Sprik, M. (1991). *J. Chem. Phys.* **95**, 6762–6769.
Stevens, E. D. (1978). *Acta Cryst.* B**34**, 544–551.
Stewart, R. F. & Spackman, M. A. (1983). *VALRAY Users Manual*. Chemistry Department, Carnegie-Mellon University, USA.
Swaminathan, S., Craven, B. M. & McMullan, R. K. (1984). *Acta Cryst.* B**40**, 300–306.
Thakkar, A. J., Koga, T., Saito, M. & Hoffmeyer, R. E. (1993). *Int. J. Quantum Chem. Quantum Chem. Symp.* **27**, 343–354.
Verhoeven, J., Dymanus, A. & Bluyssen, H. (1969). *J. Chem. Phys.* **50**, 3330–3338.